

Tumor cell directed migration based on 3D printed microfilament structure

Dongtian Zheng(郑栋天), Zhikai Ye(叶志凯), Chuyun Wang(汪楚云), Lianjie Zhou(周连杰), Xiyao Yao(姚喜耀), Guoqiang Li(李国强), Guo Chen(陈果), and Liyu Liu(刘雳宇)

Citation: Chin. Phys. B, 2025, 34 (**12**): 128703. DOI: 10.1088/1674-1056/ade424
http://cpb.iphy.ac.cn; http://iopscience.iop.org/cpb

What follows is a list of articles you may be interested in

Estimation of cancer cell migration in biomimetic random/oriented collagen fiber microenvironments

Jingru Yao(姚静如), Guoqiang Li(李国强), Xiyao Yao(姚喜耀), Lianjie Zhou(周连杰), Zhikai Ye(叶志凯), Yanping Liu(刘艳平), Dongtian Zheng(郑栋天), Ting Tang(唐婷), Kena Song(宋克纳), Guo Chen(陈果), and Liyu Liu(刘雳宇)
Chin. Phys. B, 2024, 33 (**5**): 058706. DOI: 10.1088/1674-1056/ad334c

Spatial search weighting information contained in cell velocity distribution

Yikai Ma(马一凯), Na Li(李娜), and Wei Chen(陈唯)
Chin. Phys. B, 2024, 33 (**2**): 028703. DOI: 10.1088/1674-1056/ad09d3

Characteristics of cell motility during cell collision

Yikai Ma(马一凯), Na Li(李娜), and Wei Chen(陈唯)
Chin. Phys. B, 2024, 33 (**2**): 028702. DOI: 10.1088/1674-1056/ad117c

Directional-to-random transition of cell cluster migration

Yang Zeng(曾阳), Bingchen Che(车丙晨), Dan Sun(孙聃), Ce Zhang(张策), and Guangyin Jing(经光银)
Chin. Phys. B, 2023, 32 (**11**): 118705. DOI: 10.1088/1674-1056/acf704

Diffusional inhomogeneity in cell cultures

Jia-Zheng Zhang(张佳政), Na Li(李娜), Wei Chen(陈唯)
Chin. Phys. B, 2018, 27 (**2**): 028705. DOI: 10.1088/1674-1056/27/2/028705

Tumor cell directed migration based on 3D printed microfilament structure

Dongtian Zheng(郑栋天)[1], Zhikai Ye(叶志凯)[2], Chuyun Wang(汪楚云)[4], Lianjie Zhou(周连杰)[1], Xiyao Yao(姚喜耀)[1], Guoqiang Li(李国强)[3], Guo Chen(陈果)[1,†], and Liyu Liu(刘雳宇)[1,‡]

[1] *Chongqing Key Laboratory of Interface Physics in Energy Conversion, School of Physics and Center of Quantum Materials and Devices, Chongqing University, Chongqing* 401331, *China*

[2] *Center for Theoretical Interdisciplinary Sciences Wenzhou Institute, University of Chinese Academy of Sciences, Wenzhou* 325001, *China*

[3] *College of Chemistry & Environmental Engineering, Chongqing University of Arts and Sciences, Yongchuan* 402160, *China*

[4] *Postgraduate Training Base Alliance, Wenzhou Medical University, Wenzhou* 325035, *China*

(Received 28 March 2025; revised manuscript received 3 June 2025; accepted manuscript online 13 June 2025)

Three-dimensional (3D) cell spheroids, generated utilizing the self-organizing properties of mammalian cells, exhibit significant advantages and hold important value in simulating tissue complexity. However, they still encounter numerous limitations, including the absence of spatial anisotropy in cell spheroids, which can compromise their reliability in numerous preclinical drug tests. This study utilizes two-photon polymerization (TPP) 3D printing technology, drawing inspiration from common liquid transport structures in nature, to design a microstructure featuring periodic parallel microcavities and wedge angles. This design enables unilateral immobilization and capillary rise of soft condensed matter. This structure facilitates the directed migration of 3D cell spheroids through the physical properties of the structure itself in static culture. Consequently, the original 3D cultured cell spheroids can acquire unique anisotropy within the spatial structure in a static culture environment, presenting a novel perspective for constructing biological constructs and cultivating connections between various cell spheroids, such as organoids.

Keywords: cell migration, laplace pressure, corner effect, TPP 3D printing

PACS: 87.80.Ek, 68.03.Cd, 47.55.dr, 87.85.Va

DOI: 10.1088/1674-1056/ade424 **CSTR:** 32038.14.CPB.ade424

1. Introduction

Preclinical drug experimentation is a pivotal stage in the drug development process, bridging the gap between laboratory research and human clinical trials.[1–3] Compared with the traditional two-dimensional (2D) cell model, the three-dimensional (3D) cell sphere model is closer to the in vivo microenvironment, and it plays an important role in preclinical experiments and the study of biological growth and development.[4,5] In cancer research, three-dimensional structured cancer cell spheroids can reproduce characteristics such as tumor heterogeneity, metabolic gradients, and drug resistance, in contrast to traditional 2D monolayer cell cultures.[6,7] Self-organizing 3D spheroid organoids are highly adept at recapitulating early developmental events.[8,9] However, self-organized cell spheroids lack spatial specificity in different directions. This not only increases the randomness of cell spheroid growth and development in various directions but also limits the generation of functional blocks that require specific spatial structures.[10] Therefore, while maintaining the various advantages of self-organized cell spheroids, enhancing the characteristics of 3D cell spheroids in their spatial composition through various means is undoubtedly a highly valuable issue.

Efforts have been made to improve the traditional spherical structure of three-dimensional cell spheroids.[11] Recently, a study has demonstrated that co-culturing hydrolyzable filaments generated via mechanical agitation with human pluripotent stem cells can yield embryoid bodies with a larger surface-to-volume ratio, thereby enhancing the formation of cortical plates in brain organoids.[12] Nevertheless, the length and shape of the filament structure produced by this agitation experiment are uncontrollable. Another experiment, which utilized filamentous mesh culture to generate organoid spheres, successfully promoted the formation of stem cell lumens during the process.[13] However, due to its grid-like structure, the spatial changes in this experiment are symmetrical. Additionally, structures generated by 3D printing cell technology, such as bio-ink, disrupted the early self-organization process of cells.[14,15] Therefore, there is a need for an asymmetric regulation method for cell spheroid growth and development that preserves the early self-organizing ability of cells.

We have noticed that there has always been a "quasi-fluid" phenomenon in cell populations composed of multiple cells. For example, the diffusion of glioma cells in brain tissue

†Corresponding author. E-mail: wezer@cqu.edu.cn

‡Corresponding author. E-mail: lyliu@cqu.edu.cn

© 2025 Chinese Physical Society and IOP Publishing Ltd. All rights, including for text and data mining, AI training, and similar technologies, are reserved.

conforms to the diffusion-convection equation.[16] During the gastrulation stage of zebrafish embryos, the collective migration of cells exhibits characteristics of fluid vortices and shear thinning and can be modeled using continuum mechanics.[17] Therefore, we believe that the growth of 3D cell spheroids will also be influenced, to a certain extent, by means related to the regulation of fluids.

Meanwhile, the unique microstructures evolved by plants and animals have provided valuable inspiration. They drive directional liquid movement and deformation by leveraging surface-free energy gradients and Laplace pressure gradients generated by these surface microstructures.[18–21] Upon in-depth investigation of these micro-nano structures, we found that the dimensional scales of these plant and animal surface-grown microstructures are highly similar to those of common cell scaffolds and cell spheroids. Here, we treat the entire cell mass as a soft condensed matter and attempt to regulate their growth and migration using analogous structures.

Benefiting from an advanced manufacturing technology, the two-photon polymerization (TPP) 3D printing technology leverages its capability for high-throughput fabrication of fine structures beyond the diffraction resolution limit.[22,23] We can fabricate a wedge-angle structure with a length exceeding 4 mm and a diameter of 300 μm and use it to induce directional migration of A549 cell spheroids.

In this study, we demonstrate a structure constructed via TPP 3D printing and verifying their directional transport capacity for soft condensed matter using pure water. In addition, 3D printed cell migration structures exhibited biocompatibility suitable for long-term coculture with A549 cell spheroids. On the structure, cultured A549 cell spheroids showed directional migration in the first three days, and the migration speed was affected by the wedge angle. We also found that with the extension of culture time, the increase of the surface area to volume ratio of cell spheroids, and the enhancement of the metastatic characteristics of cancer cells themselves, the cells will appear a certain non-directional reverse movement.

Finally, we improved and manufactured a new experimental structure that can accommodate multiple cell spheres to reduce the surface area volume ratio of cell spheres. This structure not only verified that the surface area-to-volume ratio would affect the performance of cell migration but also promoted the cells to move a faster and longer distance on the structure (Fig. 1).

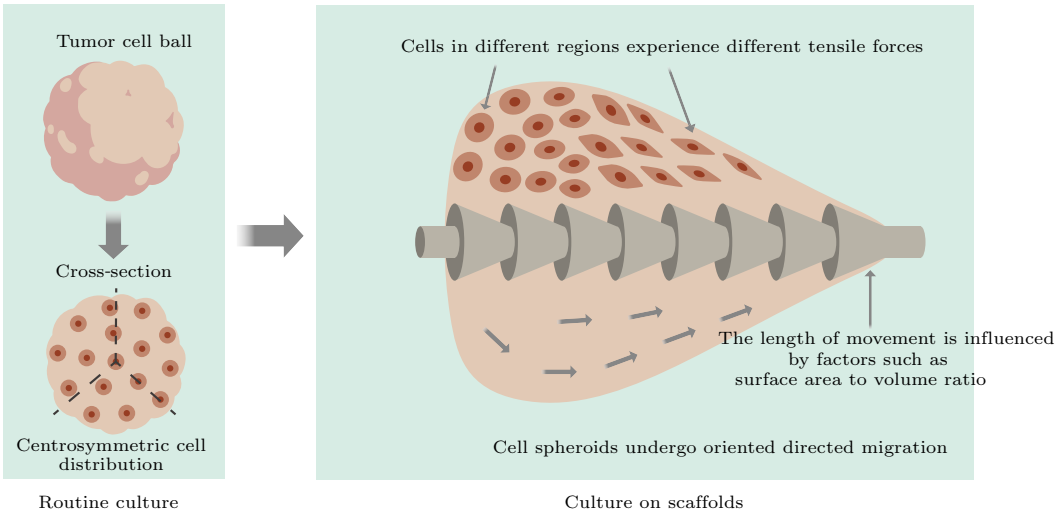


Fig. 1. Conceptual drawing of the scheme for 3D printed structures promoting directed migration of tumor cells.

2. Methods

2.1. Cultivation and preparation of A549 cells

The cells used in this study were human non-small cell lung cancer cells A549 labeled with red fluorescent protein (RFP), obtained from Zhejiang Biodi Biotechnology Co., Ltd. (Zhejiang, China). A549-RFP cells were cultured in a DMEM high-glucose medium supplemented with 10.0% fetal bovine serum (Gibco, NY, USA) and 1-μg/ml puromycin (Beyotime Biotechnology, Shanghai, China) and maintained in a 5.0% CO_2 incubator at 37.0 °C. The culture medium was replaced every three days. When the cell density reached 80% to 90%, use 0.25% trypsin/edta (Corning, New York, USA) to digest the cells and prepare a cell suspension with a density of 5.0×10^5 cells/ml for subsequent pelleting. Then, take 100 μl of cell suspension and add it into a 96-well flat bottom plate according to the amount of 5.0×10^4 cells per well for 5 days to form a cell spheroid. Add 100-μl culture medium on the first day, and then completely change 200-μl medium every two days.

2.2. Real-time cultivation of cells

In this study, a continuous recording of the cell growth status was required, so the experimental structures were cultured using the smart live cell imaging analysis system (Molecular Devices, USA) to keep a continuous record of the

experimental phenomena while maintaining cell activity. To use the smart live cell imaging analysis system, we first immobilized the cell spheroids on the structures. Here, we incubated the cells after inoculation onto the scaffold structure on a 48-well plate with an overall static incubation for 1 h to immobilize the cells. Subsequently, the lid of the live cell imaging system was opened, and the 48-well plate was placed into the culture compartment of the live cell imaging analysis system with the lid attached and closed. The culture compartment was set to be maintained at 95% humidity, 37.0 °C, and 5.0% CO_2. Cell status was recorded every ten minutes using a quadruple microscope without fluorescence excitation for 48 hours of incubation. At the end of a 48-hour phase of incubation, the 48-well plate medium was removed and completely replaced with 1 ml of culture medium and returned to the live cell device for the next phase of recording and incubation.

2.3. Preparation of the 3D-printed structure

The 3D printed microstructures in this study were fabricated using two-photon polymerization (TPP) 3D printing and IP-Q photoresist (Nanoscribe, Germany). Auto CAD software (2016, Autodesk) was used to design the 3D models required for the experiments, and the files were subsequently exported to .stl format and imported into the printer's corresponding slicing software, Describe (Nanoscribe, Germany), for slicing parameter settings. Here, we used the parameters of 5-μm line width and 15° splicing angle for multi-block printing and splicing of the structure, which was then exported as a printer work file in .job format. Next, we drop a suitable amount of photoresist onto the silicon substrates (Nanoscribe, Germany), blow and make sure that there are no air bubbles, put the substrate with photoresist into the printer, and import the designed work file into the printer for printing. After printing, the substrate was removed and immersed in 99.5% propylene glycol methyl ether acetate (McLean, China) for 15 min to remove the excess photoresist. The printed structure was then immersed again in 99.9% isopropyl alcohol (McLean, China) to remove the propylene glycol methyl ether acetate from the previous step. After completing the above operations, the 3D printed structures were peeled off from the substrate and placed into a 25-mm cell culture dish filled with 70% alcohol for overnight immersion to increase the cytocompatibility of the structures.

2.4. Design and fabrication of the 3D-printed structure

To drive the migration of cell spheroids on the 3D printed structures, we designed and fabricated (Fig. 2(a)) hemline-shaped cell directed migration structures with two different angles, and a set of smooth parallel controls, as shown in the figure (Fig. 1(b)), concerning the sizes of common cell spheroids and the dimensions of fluid transport structures in nature. The whole model consists of three parts: two side-by-side bionic wedge-angled filament structures, baffles with beveled angles on both sides of the filament structures to help the cell spheres to orient themselves, and a whole base structure.

After completing the design of the printed structure we fabricated the structure using a two-photon 3D printing system. The printed structures were examined using field emission scanning electron microscopy and body microscopy (Figs. 2(c)–2(e)). It was confirmed that they met our design specifications.

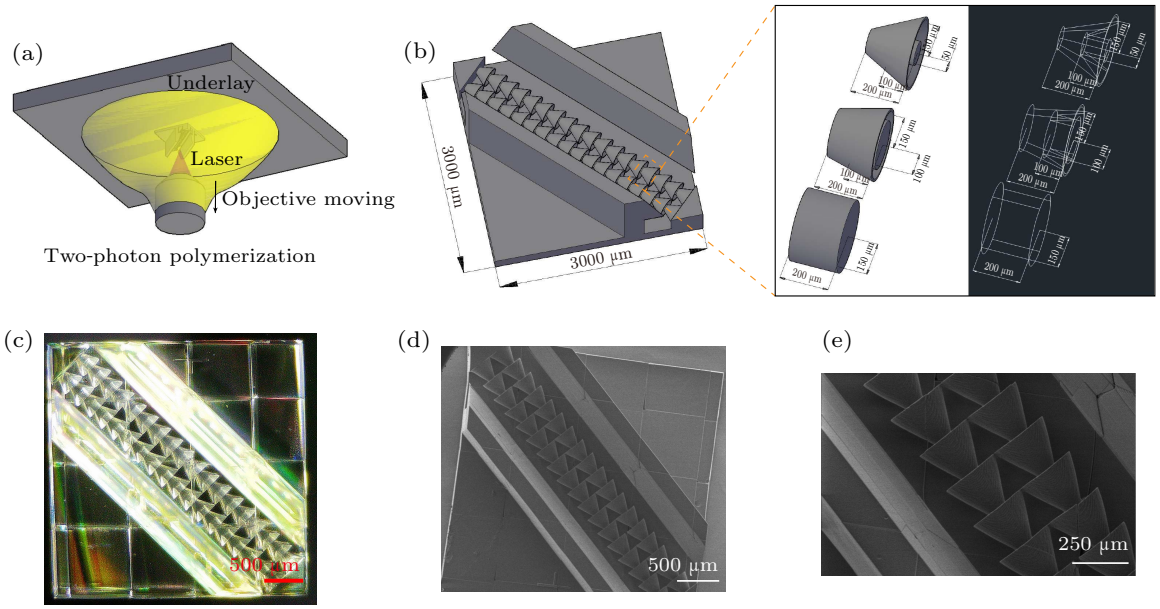


Fig. 2. Fabrication and characterization of 3D printed structures: (a) schematic diagram of the production process of 3D printed structures using TPP 3D printing. The corresponding 3D printed structures were obtained after two-photon polymerization and photoresist development, (b) schematic diagram of the 3D printed cell migration structure concerning the dimensions of the bionic droplet transport structure where two wedge angle structures and a smooth control were designed, (c) bright field images of the 3D printed structures with a scale bar of 500 μm. (d) and (e) Scanning electron microscope images of the printed structures to confirm that they meet our design specifications.

3. Results and discussion

3.1. Functional verification of 3D printed microfilament structures

In the microfilament structure with a hemline-shaped structure designed in this experiment, we expect that the soft condensed matter receives multiple physical driving forces. The first one is the Laplace pressure difference generated by the conical structure with asymmetric axial radius, where the liquid is driven to transport from the high curvature measure to the low curvature measure under the action of this force (Fig. 3(a)).[24] The Laplace force can be expressed as

$$F_{\text{Laplace}} = -\int_{R_2}^{R_1} \frac{2\gamma}{(R+R_0)^2} \sin\alpha \, \mathrm{d}z, \tag{1}$$

where γ is the surface tension of the liquid, R is the local radius of the vertebrae, R_1 and R_2 are the local radii of the droplet relative to the vertebrae on both sides, and R_0 is the radius of the droplet. α is the half-vertex angle of the vertebrae, and $\mathrm{d}z$ is the minute incremental radius along the vertebrae.

Meanwhile, in the perpendicular direction of the chamber formed by each hemline-shaped structure and the central connecting cylinder, the liquid is subjected to capillary rise action. The height of its capillary rise can be calculated in terms of the balance between gravitational and interfacial potentials.[25] It can be expressed as

$$H(x) = \frac{2\gamma\cos\theta}{\rho g x \alpha_1} + \frac{\alpha_1 - \alpha_2}{\alpha_1 h} H^2(x), \tag{2}$$

where γ, ρ, θ, α, g, h, and $H(x)$ represent liquid surface tension, liquid density, contact angle, opening angle, gravitational acceleration, height of the intersecting structure, and liquid level height at position x.

Here, we localize the low curvature side of the filament structure in the forward direction. From the cross-section of the filamentary structure, for a periodically arranged wedge, capillary forces within each of its small structures drive the forward movement of the liquid. At the same time, in the opposite direction, the movement of the liquid is stopped due to the pinning effect. Specifically, the sharp edge structure leads to immobilization of the liquid when the apparent contact angle θ of the liquid is less than $\pi - \phi + \theta_0$, where θ_0 and ϕ are the intrinsic contact angle and the angle of the liquid at the sharp edge.[26,27]

As we can see from the design diagram, on the single hemline-shaped structure we designed, the soft matter is subjected to the Laplace pressure difference generated by the asymmetric structure of the axial radius, which promotes its movement toward the low curvature side. Filamentary structures composed of multiple structures it is subject to pinning effects at the sharp edges, preventing them from moving in the reverse direction. In chambers composed of structural hems the structures themselves are in turn driven by capillary rise, filling the entire chamber rapidly in the forward direction. Given these two forward-movement-promoting structures and one reverse-motion-stopping structure, we expect that the liquid matter can achieve forward-directed movement on the structure without external energy input under the combined effect of the Laplace pressure difference due to the angular effect and the pinning effect of the capillary rise force.

Pure water was then used to test the functionality of the structure. The structures chosen for testing were the filament structure with the largest wedge angle and the smooth control manufactured in Subsection 2.4. Specific parameters can be found in Fig. 2(b). A syringe pump was used to pump liquid into the center of the structure at flow rates of 24 μl/min and 9 μl/min to examine the functionality of the filamentous structure by observing the specific movement of the liquid. Here we placed the structure on a microscope stage and recorded the phenomenon of liquid movement on the structure by an external high-speed video camera (Ametek, USA) (see Fig. 3(b)).

Images were taken of the motion of the liquid over the structure over time. By observing the experimentally recorded images, we can find that, unlike the smooth parallel structure, the motion of the liquid on the thin filamentary structure with hemline-shaped wedge angles is oriented and shows unilateral movement. Whereas on the smooth contrasting structures, the tendency of the liquid to spread to both sides is roughly the same (Fig. 3(c)).

Meanwhile after we have normalized the relationship between the unilateral liquid transport distance with time (Fig. 3(d)). It can be seen that the proportionality between the velocity of liquid movement on the structure and the velocity of liquid injection by the syringe pump on a smooth plane does not correspond exactly. It is considered here that it may be the orifice of the pipe transporting the liquid was not affixed to the structure at the beginning of the experiment, resulting in a certain amount of liquid hanging in the orifice before the start of the movement. Comparing the movement of the liquid on the hemline-shaped wedge angle structure at the same syringe pump liquid flow rate, we find that the liquid is moving in one direction on the hemline-shaped structure, but the overall velocity is still less than its smooth control moving in both directions. By observing the pictures of the liquid movement and analyzing the design of the two structures, we analyze that this may be the liquid needs to fill the chamber on the directional movement structure, as well as receiving the influence of lateral diffusion on the hemline-shaped structure, the volume of movement per unit distance is greater. However, in general, the filamentary structure with a hemline-shaped wedge angle is capable of directional transport of the fluid substance.

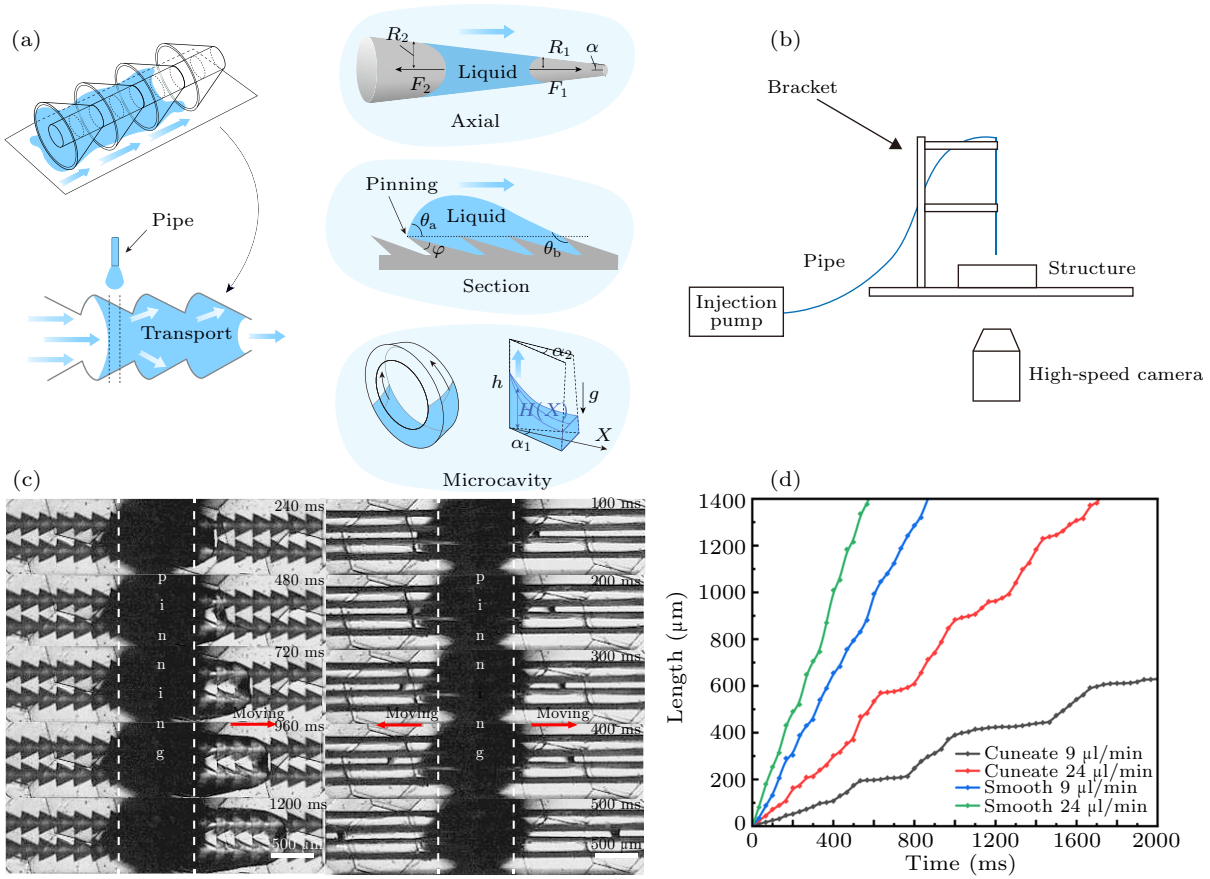


Fig. 3. Experimental diagrams of liquid movement under microscope: (a) schematic diagram of the principle of force on liquid movement in the structure, (b) installation diagram of the whole droplet experiment, (c) picture of continuous liquid movement under inverted microscope. Where the syringe pump flow rate was 24 μl/min, (d) statistical diagram of the maximum distance of liquid movement on the control and filament structures at two different flow rates.

3.2. Migration experiment of cells on 3D printed filament structures

In the cellular experiment section, it was observed whether the cell spheres could act as a fluidic substance subjected to the force generated by the structure by inoculating the cell spheres onto the 3D printed microstructures. The following is the general flow chart of this experiment (Fig. 4(a)). Firstly, for cells, we chose the cultured A549 cell spheroids from the experimental methods section. After five consecutive days of culturing, we obtained rounded cancer cell spheroids with a diameter of around 650 μm. Subsequently, a pipette gun with a wide-mouth tip was used to move them to the middle of the two filaments of the 3D-printed structure placed in a 48-well plate (Fig. 4(b)). Then, we use the smart live cell imaging analysis system for continuous culture and observation.

As we can see from the photographs taken by the smart live cell imaging analysis system (Fig. 4(c)). For the migrated structure with a wedge angle of about 26.6°, there was no significant cell crawling out in the reverse direction and relatively good cell migration in the axial forward direction. For the structure with a smaller wedge angle of about 14.0°, the cell crawling out in the antiaxial direction was weaker and mostly migrated in the forward direction in the first 24 h but still showed significant cell migration in the antiaxial direction with the extension of time. As for the smooth contrast structure, there was obvious cell migration in both axial and antiaxial directions, and the performance of migration was more consistent. For the smaller angle of 14.0°, the restriction of cell movement was only observed at the early stage of the experiment, and the trend of forward and reverse movement was not obvious. However, for the larger angle of 26.6°, the directional movement of the cells was evident. Here, we consider the smaller wedge angle pinning effect to be due to the more stringent requirements on the contact angle between the cell and the structure, as well as the relatively small Laplace pressure difference. Overall, however, the directed migration of cells can be achieved on 3D printed microfilament structures with a certain wedge angle.

The length of cell migration within 36H was measured using ImageJ software (Fig. 4(d)). Based on the statistical results, it can be seen that for the wedge-shaped cell directional migration structure with a slightly larger angle (about 26.6°), the overall directional migration of cells was faster overall than the structure with a slightly smaller angle wedge-shaped structure (about 14.0°). The small-angle wedge structure was slightly faster than the smooth parallel structure. Overall, a wedge with an appropriate angle not only prevents the cells

from moving in the anti-axial direction but also facilitates the acceleration of cell movement in the axial direction within a certain period.

Edge analysis was done on the edges of the cells of the 3D cell spheres on the 26.6° wedge angle structure (Fig. 4(e)), where we can visualize the positive movement of the cells over time, and the increase in the cross-sectional area of the cells in the whole horizontal plane with the increase in incubation time. At the same time, we also noticed that as the incubation time increased, discrete cells appeared in the structure at 72h, and a large number of discrete cells appeared after 84 h of incubation. Based on the speculation, we believe that the cancer cell spheroids showed a more invasive state as the incubation time increased. This may have an adverse effect on our experiments.

In contrast to the previous graphs of the results of the droplet transport experiments, the directional flow rate of the liquid at the same syringe pump flow rate in the droplet transport experiments is less than the cell migration rate on the smooth structure. The reason for this is due to the difference in the volume required per unit length of movement. However, in the cellular experiments, the directional movement speed of the cells was greater than that of the smooth structure. Here, we think that it may be caused by the different forms of cell and fluid movement in the structure. In the smooth control, the cells were migrating along the entire rod, whereas the liquid was mainly in the middle of the two rods, showing a capillary rise. However, it is also possible that the directional migration structure biologically induces the directional migration of the cells to some extent. For example, it promotes the formation of new focal contacts for cancer cells.

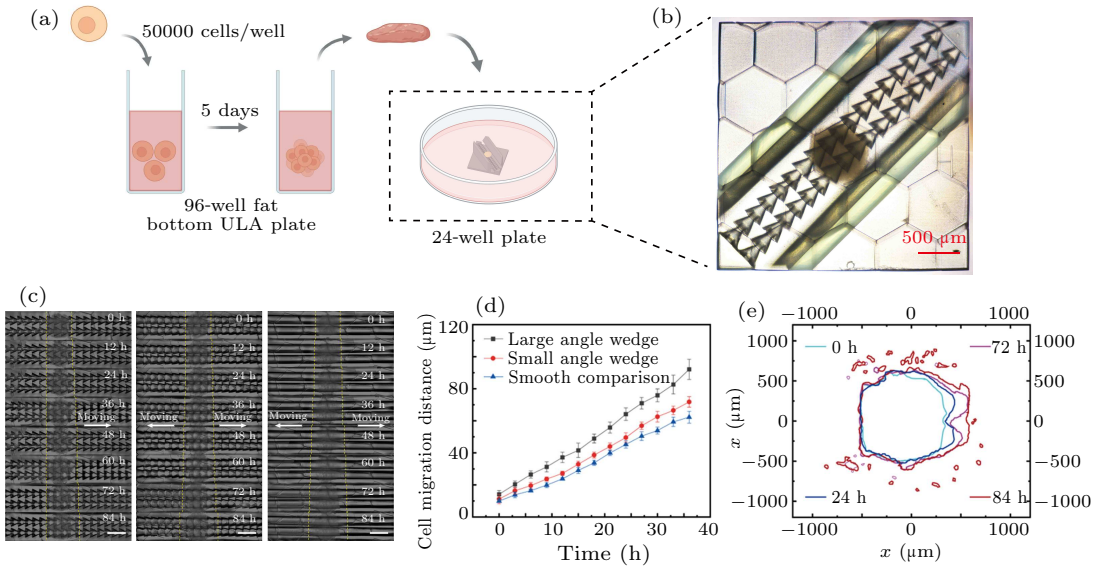


Fig. 4. Experimental diagram of a single cell sphere moving on a structure: (a) schematic representation of cells from culture to inoculation on a directionally migrating structure, (b) inverted microscope of a structure inoculated with cell spheroid, (c) migration of cells over 84 h recorded by live cell microscopy. The scale bar is 500 μm. (d) Distances traveled by cells toward the farthest end of migration at three different angles (26.5°, 14.04°, and 0° smooth contrast) were analyzed, (e) edge analysis identifies the boundaries of the A549 sphere on the 26.6° wedge angle structure at 0 h, 24 h, 72 h, and 84 h.

3.3. Improvement of structure and migration of multicellular spheres

Although it is in the experiments, the cell appeared to migrate directionally on the designed 3D printed filament-like structures. However, the cell moves relatively short distances, and it is difficult to accomplish the long-range connections between cell spheroid required in some biological constructs by promoting the growth of a long protruding structure from the cell spheres.

At the same time in with the prolongation of the culture time, we found that some anti-axial migration of cells also appeared on the well-directed migrating structures in the long-time culture (Fig. 5(a)).

For the reverse movement that occurs in these prolonged cultures, we hypothesized that the reason for the occurrence is related to the increased surface area to volume ratio due to the spreading of cells on the scaffold. Since the physical gradient of the structure is provided by the Laplace pressure difference generated by the asymmetric liquid surface, a larger surface area-to-volume ratio would undoubtedly reduce the physical gradient to which the cells are subjected and allow the unoriented movement of the cells themselves to dominate. To validate this hypothesis, we conducted an analysis of the trend of cells moving in the opposite direction. For ease of description, we define the ratio of the cross-sectional area of cells moving in the backward direction (S_b) to that of cells moving in the forward direction (S_f) identified at the boundary as the free tendency of cell migration, k. The magnitude of k mainly reflects the occurrence of non-directional cell movement: the larger k is, the more obvious the non-directional movement becomes, whereas a smaller k indicates better directional move-

ment. Meanwhile, through observing cells, we found that as the area occupied by cells on the scaffold increases, the overall transparency of the cell mass improves and becomes thinner. Therefore, we believe that changes in the total cell area are positively correlated with the surface area-to-volume ratio of cells to a certain extent. Compared with using time as the horizontal axis, due to the proliferation of cells themselves, the proliferation of cells increases within the same time period as the culture time extends, leading to faster changes in area within the same time period and intensified data changes in the second half, which is not conducive to the analysis of the fundamental relationships. Therefore, we use the total horizontal area of cells as a reference for the surface area-to-volume ratio to observe the changes in the free tendency of the cell migration.

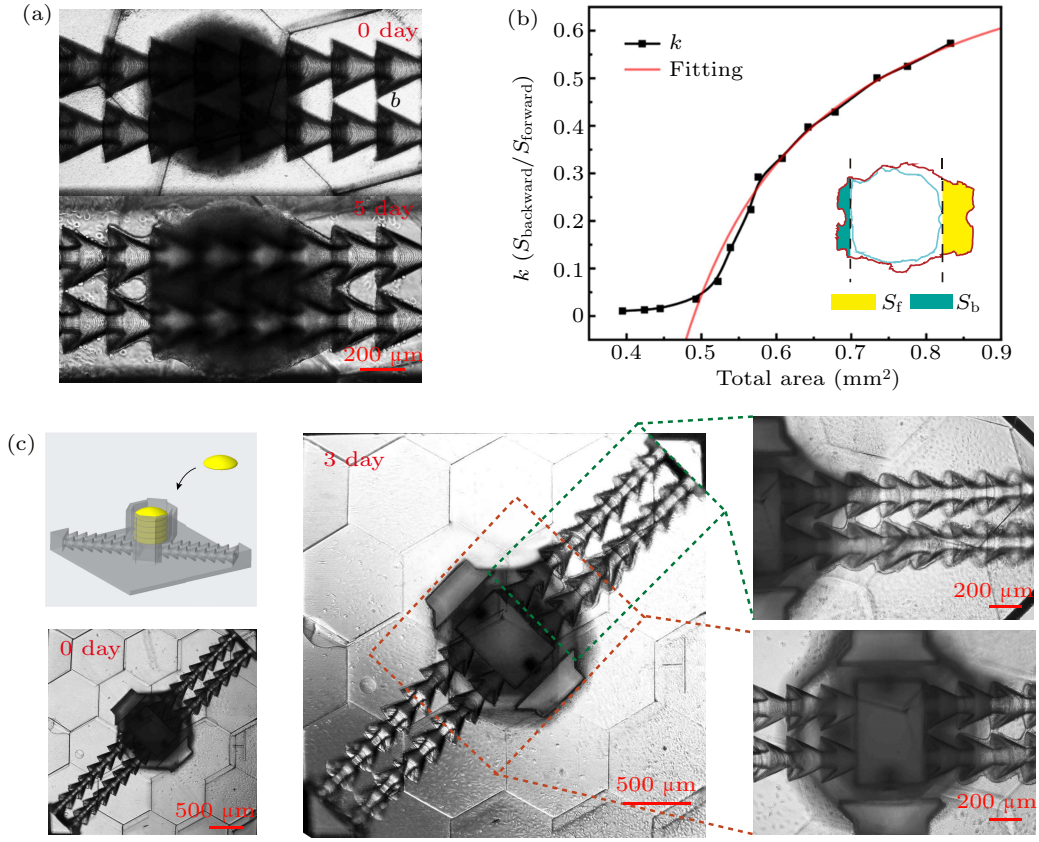


Fig. 5. Schematic diagram of the migration experiment with more cells superimposed: (a) with the extension of time the cells show some anti-axial movement, (b) the tendency of cell movement changes with the variation in total area, (c) the structural design for loading more cells, along with the movement of cells cultured on this structure for three days, revealed that the cells migrated faster and farther with no reverse movement.

From the statistical results, it can be seen that with the increase of the total area, the ratio of the backward area to the forward area of the cells gradually increased, and the ability of directional migration became weaker. When the total cell area was less than 0.5 mm^2, the free tendency of cell migration was close to 0, which showed good directional movement characteristics. As the total area increased, the free tendency of the cells firstly appeared to increase significantly, and then the growth trend gradually became smooth. Considering that the second half of the curve after the emergence of free movement behaves similarly to an arc upward converging function, we made assumptions about the movement of the second half of the curve with a variety of models and did curve fitting, among which the best results were obtained after fitting the curve with the following formula:

$$f(x) = \frac{a(x-b)}{(x-b)+c}, \tag{3}$$

where $(x-b)$ is the area of forward movement after reverse migration occurs, a is the ratio of the reverse and forward movement velocities, and we assume that there may be a proportional relationship between the two velocities when the movement reaches equilibrium, b is a correction for the initial area of the cell, and c is the area of forward movement when only forward movement occurs. The value of a in this model is about 0.90 after retaining two decimal places, b is about 0.49, and c is about 0.20, and the coefficient of determination R^2 is calculated to be 0.9876, which is a good fit. According to the formula, it is presumed that after the cell appears to move in the reverse direction, the speed of the movement will increase abruptly in a short time, catch up with the speed of the forward movement, and remain in a state that tends to stabilize, but by the promotion of the forward movement by the structure itself, the speed may still be slightly smaller compared to the forward movement, which is about 0.9 times of the rate of the forward

movement. At the same time, as the movement time becomes longer, $(x-b)$ becomes larger while the value of c remains constant, and eventually the overall ratio will converge to a. (Fig. 5(b))

A new structure was then designed for experimental validation, which differed from the previous structure by placing five A549 cell spheroids in the same initial area (Fig. 5(c)). From the experiments, it can be seen that our newly designed structure with smaller surface area-to-volume ratio demonstrated stronger directional cell migration compared to the previous single cell spheroid with larger surface area-to-volume ratio, with four nodes crawling out in the forward direction in three days of incubation, while no reverse crawling was observed (Fig. 5(d)). This verified our previous assumptions.

4. Conclusion

In this 3D microfilament structure-induced directional migration experiment of cell spheroid, we took reference from bionics and designed a directional transport structure for soft condensed matter concerning the principle of liquid directional transport bionic structure, which is relatively mature at present. In this experiment we first verified the directional transport ability of the designed structure for liquid substances by pure water. After determining that the structure was able to exhibit our functional expectations, we performed co-culture experiments of the structure with an A549 cell spheroid. The results showed that the printed structure with a wedge angle of 26.6° had a good effect on inducing directional migration of 3D cell spheroids, with almost no counter-axial movement of the cells observed in the first 72 h. At the same time, quantitatively comparing the directional transport of droplets, we found that the effect of the filament structure on the directional transport of cell spheroids was similar or even better than that of droplets for a certain period. We also discussed and conducted secondary experiments on the possible causes of the anti-axial movement of cells in extended cultures. It was verified that smaller surface area-to-volume ratios help cells exhibit more pronounced directional migration phenomena in the structure.

Overall, this study designed a 3D-printed cell-guided migration structure and validated its functionality through co-culture with cell spheroids while discussing key phenomena observed in cell migration experiments. In the future, the designed cell-guided migration filaments may enable interconnection between multicellular spheroids, providing a novel direction for the development of multi-organ chips and the construction of complex physiological environments. Furthermore, by leveraging differential adhesion mechanisms among various cell types, our structure could potentially regulate the spatial distribution of cells within spheroids. Additionally, the impact of filament structures on cancer cell spheroid migration may offer insights for studying cancer metastasis in complex microenvironments.

Acknowledgements

Project supported by the National Natural Science Foundation of China (Grant Nos. T2350007 and 12174041), the Natural Science Foundation of Chongqing (Grant No. CSTB2024NSCQ-MSX0596), the Science and Technology Research Program of Chongqing Municipal Education Commission (Grant No. KJZD-K202401306), and the Scientific Research Fund of Chongqing University of Arts and Sciences (Grant Nos. R2023HH03 and P2022HH05).

References

[1] Sowah M N, Klein B R, Lu V M, Komotar R J and Levi A D 2025 *Neurosurg. Rev.* **48** 294
[2] Dmour I 2025 *J. Pharm. Innov.* **20** 44
[3] Qader M A, Hosseini L, Abolhasanpour N, Oghbaei F, Maghsoumi-Norouzabad L, Salehi-Pourmehr H, Fattahi F and Sadeh R N 2025 *BMC Neurosci.* **26** 17
[4] Lee S Y, Koo I S, Hwang H J and Lee D W 2023 *SLAS Discov.* **28** 119
[5] Patel T and Jain N 2024 *Life Sciences* **358** 123184
[6] Yao J, Li G, Yao X, Zhou L, Ye Z, Liu Y, Zheng D, Tang T, Song K, Chen G and Liu L 2024 *Chin. Phys. B* **33** 058706
[7] Brancato V, Oliveira J M, Correlo V M, Reis R L and Kundu S C 2020 *Biomaterials* **232** 119744
[8] Clevers H 2016 *Cell* **165** 1586
[9] Lancaster M A, Renner M, Martin C A, Wenzel D, Bicknell L S, Hurles M E, Homfray T, Penninger J M, Jackson A P and Knoblich J A 2013 *Nature* **501** 373
[10] Pasca S P 2018 *Nature* **553** 437
[11] Baptista L S, Mironov V, Koudan E, Amorim E A, Pampolha T P, Kasyanov V, Kovalev A, Senatov F and Granjeiro J M 2024 *Tissue Eng. Part A* **30** 377
[12] Lancaster M A, Corsini N S, Wolfinger S, Gustafson E H, Phillips A W, Burkard T R, Otani T, Livesey F J and Knoblich J A 2017 *Nat. Biotechnol.* **35** 659
[13] Ritzau-Reid K I, Callens S J P, Xie R, Cihova M, Reumann D, Grigsby C L, Prados-Martin L, Wang R, Moore A C, Armstrong J P K, Knoblich J A and Stevens M M 2023 *Adv. Mater.* **35** 2300305
[14] Kačarević ŽP, Rider PM, Alkildani S, Retnasingh S, Smeets R, Jung O, Ivanišević Z and Barbeck M 2018 *Materials* (Basel) **11** 2199
[15] Xu H Q, Liu J C, Zhang Z Y and Xu C X 2022 *Military Medical Research* **9** 70
[16] Engwer C and Wenske M 2021 *J. Math. Biol.* **82** 10
[17] Betz T 2021 *Viscoelasticity and Collective Cell Migration* (London, San Diego, CA: Elsevier) pp. 135–155
[18] Zheng Y, Bai H, Huang Z, Tian X, Nie F Q, Zhao Y, Zhai J and Jiang L 2010 *Nature* **463** 640
[19] Ju J, Bai H, Zheng Y, Zhao T, Fang R and Jiang L 2012 *Nat. Commun.* **3** 1247
[20] Nørgaard T and Dacke M 2010 *Front. Zool.* **7** 23
[21] Feng L, Li S, Li Y, Li H, Zhang L, Zhai J, Song Y, Liu B, Jiang L and Zhu D 2002 *Adv. Mater.* **14** 1857
[22] Han F, Gu S, Klimas A, Zhao N, Zhao Y and Chen S C 2022 *Science* **378** 1325
[23] Zhu W, Ma X, Gou M, Mei D, Zhang K and Chen S 2016 *Current Opinion in Biotechnology* **40** 103
[24] Renvoisé P, Bush J W M, Prakash M and Quéré D 2009 *Europhys. Lett.* **86** 64003
[25] Chen H, Zhang P, Zhang L, Liu H, Jiang Y, Zhang D, Han Z and Jiang L 2016 *Nature* **532** 85
[26] Oliver J F, Huh C and Mason S G 1977 *Journal of Colloid and Interface Science* **59** 568
[27] Li J and Guo Z 2018 *Nanoscale* **10** 13814